Eur. Phys. J. Appl. Phys. (2014) 65: 11101
DOI: 10.1051/epjap/2013130340

THE EUROPEAN PHYSICAL JOURNAL
APPLIED PHYSICS

Regular Article

Light transmission measurement of solute dispersion in non-Brownian suspension flow

Alejandro Boschan[a], Mariana Poblete[b], Yanina Lucrecia Roht, Irene Ippolito, and Ricardo Chertcoff

Grupo de Medios Porosos and CONICET, Facultad de Ingeniería, Universidad de Buenos Aires, Paseo Colón 850, 1063 Buenos Aires, Argentina

Received: 22 July 2013 / Received in final form: 1 October 2013 / Accepted: 22 October 2013
Published online: 6 January 2014 –

Abstract. We characterize and employ a light transmission technique to measure the dispersivity of a solute in the flow of a neutrally-buoyant non-Brownian spherical particle suspension in a Hele-Shaw cell (parallel-plate axial flow). Particle radii (a) were 20 and 40 μm, the particle bulk volume fraction ϕ_{bulk} was 0.2, and the cell aperture was 420 ± 10 μm. In each displacement experiment a suspension with a colouring solute displaces a transparent one at constant flow rates ranging from 0.721 to 0.928 mL/min (corresponding to solute Péclet numbers (Pe_{s}) between 350 and 450). A reference measurement, identical to the displacement ones but without particles in the flow ($\phi_{\text{bulk}} = 0$), were performed in the same experimental assembly for comparison purposes. A light calibration related the transmitted intensity I to the solute concentration c for each combination of ϕ_{bulk} and a. The time variation of the solute concentration was found to be well-fitted by the solution of the advection-dispersion equation (ADE) in the range of Pe_{s} studied, and consequently a dispersion coefficient D and a dispersivity l_{d} of the solute were measured.

1 Introduction

Suspension flow involving particle but also solute transport takes place in a range of environmental applications and industrial processes such as chemical waste management or exploitation of hydrocarbon reservoirs. The influence of many factors needs to be clarified in order to achieve an accurate description of both suspension dynamics and solute dispersion mechanisms, i.e., flow conduit geometry, properties of the carrier fluid, size distribution, shape and density of the particles, diffusive and adsorptive properties of the solute.

Recently, the flows of colloidal and non-colloidal (or macroscopic) particle suspensions, with particles sizes smaller or greater than 1 μm respectively, have been studied by many authors, basically because of the development of an important number of applications (coatings and food industry, perforation fluids, sediment transport), and also because new experimental techniques are available, such as confocal microscopy [1] or NMR [2,3]. These new techniques allow one to investigate suspension microstructure and rheological properties in detail. Both have also been studied extensively from the numerical point of view [4,5].

On the other hand, transport and dispersion of solutes in subsurface flow have been subject of research for many years [6,7], mainly because of subsurface contamination issues. In subsurface flow, the phase carrying the solute is often modeled as a single fluid with given viscous properties (aqueous solutions, polymers) flowing at low flow Re number, or eventually as a multiphase flow for example in hydrocarbon related applications. The geometry of the media plays in all cases a crucial role in the dispersion of the solute [8–10].

Frequently, in environmental and industrial applications, solute dispersion occurs in a two-phase flow, composed by a solid (particulate, unconsolidated) phase in addition to the fluid one. The presence of this solid phase adds complexity to the phenomenon of solute transport and dispersion, mainly because the flow of a suspension is much harder to describe than that of a pure fluid. Particle micro-organization and migration may modify the local and global properties of the flow thus affecting in turn the dispersion of the solute.

Previous works mainly addressed the differential transport of solutes and colloidal particulate material.

Massei et al. [11] studied transport and deposition of quartz particles relative to dissolved fluorescein in experiments performed in a highly permeable porous media. A retardation of the particles with respect to the solute was measured, with higher dispersivity for the latter.

Zvikelsky and Weisbrod [12] studied the impact of particle size on colloid transport in natural fractured media relative to Li^+ and Br^- as soluble tracers. In this case, on the contrary, the particles showed earlier arrival times than the solute and an advective-dominant transport behavior.

[a] e-mail: aboschfi@gmail.com
[b] The first two authors have contributed equally to the work.

Reno et al. [13] studied dispersion of colloidal carboxylate microspheres and chloride as a solute in synthetic fractures, with a near breakthrough behavior between colloids and solute. They found a dependence of colloid dispersion on the flow rate and the fracture length but not an evident one on the particle size.

Zheng et al. [14] studied numerically the differential transport and dispersion of colloid particles and molecular scale solutes in constant and variable aperture fractures, finding the conditions for which Taylor dispersion and its extension for finite-colloid size can describe accurately colloid and solute dispersion.

In a previous work, Roht et al. [15] measured the longitudinal dispersion coefficient D of a passive solute in the Poiseuille, parallel-plates, flow of a macroscopic suspension, for a range of particle bulk volume fractions (ϕ_{bulk}) and flow rates (quantified by the solute Péclet number Pe_{s}). They found a decrease of D for $\phi_{\text{bulk}} > 0.15$ and $Pe_{\text{s}} > 300$ compared to $\phi_{\text{bulk}} = 0$, implying that the presence of the particles may reduce the dispersion of the solute in this flow configuration.

1.1 Solute dispersion in simple fluid flows

In general, the dispersion of a tracer or solute is due to the combination of the molecular diffusion and the spatial variations of the flow velocity. In the case of a smoothly varying and weakly fluctuating permeability field, the solute concentration satisfies the classical macroscopic advection-dispersion equation (ADE) [16].

Moreover, in simple flow configurations such as flow between infinite parallel-plates, the variation of the longitudinal dispersion coefficient D with the mean velocity is given by equation (1) [17,18]:

$$\frac{D}{D_{\text{m}}} = 1 + \frac{Pe_{\text{s}}^2}{210}; \qquad Pe_{\text{s}} = \frac{\text{d}U}{D_{\text{m}}}; \tag{1}$$

where d is the typical distance across the flow, and D_{m} is the molecular diffusion coefficient. For flow in a cylindrical capillary tube the factor 1/210 changes to 1/48. This type of dispersion is known as Taylor dispersion, and it is achieved after sufficient time to allow transverse solute diffusion to homogenize the concentration in the direction perpendicular to the mean flow (cf. Sect. 3).

The Péclet number of the solute, Pe_{s}, characterizes the relative influence of the molecular diffusion of the solute and of its advective transport. A distinction should be made with particle Péclet number Pe_{p} to be defined in Section 1.2.

As Pe_{s} increases the term due to molecular diffusion becomes negligible and D, and the dispersivity $l_{\text{d}} \equiv D/U$; vary as

$$\frac{D}{D_m} = \frac{Pe_{\text{s}}^2}{210}; \quad l_{\text{d}} = \frac{Pe_{\text{s}} d}{210}; \tag{2}$$

In heterogeneous media with a strongly fluctuating permeability field, geometrical dispersion and macrodispersion [19] may exist.

1.2 Suspension flow

Flowing behavior of suspensions have been extensively studied in numerous theoretical, numerical and experimental works.

The particle Péclet number $Pe_{\text{p}} = \frac{6\pi\mu_0 a^3\dot{\gamma}}{kT}$ and the particle Reynolds number $Re_{\text{p}} = \frac{\rho_0 a^2\dot{\gamma}}{\mu_0}$ provide a measure of the relative magnitude of viscous and Brownian effects and of inertial and viscous effects respectively (here a is the particle radius, $\dot{\gamma}$ the characteristic shear-rate, ρ_0 the density of the particle, μ_0 the viscosity of the solvent, k Boltzmann's constant and T the absolute temperature). In Section 7 we shall see that the values of these parameters in the present work imply very high Pe_{p} and very low Re_{p}.

In the case of negligible Brownian and inertial effects, fluid-particle and particle-particle interactions are then mostly driven by viscous stresses.

There is consensus about the fact that, in many flow situations, the stationary spatial distribution of the particles may be inhomogeneous [20,21]. This makes the description of the suspension as an effective fluid complex [22]: the microstructure of the suspension becomes of extreme importance, especially as ϕ_{bulk} increases. For example, it has been shown that, even at low ϕ_{bulk}, suspensions may present chaotic behaviour [23].

In particular, particle migration to low shear zones due to shear-induced diffusion [24,25] may strongly modify the velocity field. In simple axial flows (parallel-plates, cylindrical and rectangular channels), the shear induced diffusion causes the particles to migrate to the centre of the channel. This results in an local increase of ϕ and a blunting of flattening of the velocity profile [2,20,26]. This phenomenon has been explained [5] by a local increase of the viscosity associated to the local increase of ϕ, and has been observed for ϕ_{bulk} as low as 0.05 [1] (we follow the nomenclature of this author by using ϕ for the local particle volume fraction and ϕ_{bulk} for the bulk or large scale one).

The modification of the velocity profile in the channels due to shear-induced migration may presumably affect the dispersion of a solute.

2 Experimental methods

2.1 Fluid and suspension preparation

Neutrally-buoyant suspensions were prepared using a Newtonian carrier fluid containing 21% in weight of glycerol in water (aprox. 1.05 g/cm^3).

This solution is fractioned in two equal parts, and then the solute (Waterblue colorant [27]) is added to one part (2.0 g/L), and NaCl to the other (2.0 g/L). The latter is added in order to match densities and avoid gravity-driven instabilities between the carrier fluids of a coloured displacing suspension and a transparent displaced suspension used in the displacement experiments.

A small drop of surfactant (SDS) is also added to each part in order to improve the wettability; finally an identical quantity of spherical particles (Dynoseeds

TS40 or TS80, radii a: 20 ± 1 and 40 ± 2 μm, density: 1.05 g/cm^3) is added to each part in order to obtain $\phi_{\text{bulk}} = 0.2$.

Coloured and transparent carrier fluid without particles is reserved for the auxiliary reference experiments.

Deviations from neutral buoyancy, detected visually, were corrected by adding small drops of water or glycerol simultaneously to both coloured and transparent fractions.

The suspensions were left in observation in an elongated bottle for at least 3 days before performing the experiments to check neutral-buoyancy. We estimated that the presence of a layer of clear fluid at the top or at the bottom of the suspension (due to buoyant particles moving up or down) could be determined with reasonable accuracy by direct inspection if the layer has at least a thickness of 0.5 cm. A displacement of 0.5 cm in 3 days would correspond to a displacement of 0.003 cm (less than a tenth of the measured cell aperture d, cf. Sect. 2.4) in the typical duration of our longest experiments (20 min). As temperature plays a crucial role in the buoyancy of the particles, room temperature (24 °C) was controlled by air conditioning and verified by a regular thermometer during the buoyancy tests and experiments.

Also, in the same way that described above, suspensions with pattern solute concentrations 0; 0.4; 0.8; 1.2; 1.6 and 2 g/L were prepared for the auxiliary light calibration measurement that will be described in Section 2.5.

2.2 Light transmission technique for pure fluids

The technique used in this work to measure solute concentration in suspension flow is an extension of that used in previous works [28,29] for fluid flow (with no macroscopic particles) in constant and variable aperture fractures. The technique makes use of an auxiliary light calibration that allows one to determine the functional relation between the concentration c of a colouring, light-absorbing solute, dissolved in a layer of fluid, and the transmitted intensity (I) through the latter. The explicit form of this relation is later used to determine the unknown c from the measurement of I in the main displacement experiments.

Consider c, $c_{\min}$ and $c_{\max}$ being respectively the unknown, minimum and maximum solute concentrations dissolved in the (otherwise transparent) fluid saturating the cell; and I, $I_{\max}$ and $I_{\min}$ the corresponding transmitted intensities. We assume here that the aperture d of the cell is constant.

With the use of an extended Beer-Lambert law, the transmitted intensity I can be written as:

$$I = I_{\max} \exp\left(-\mu f_1(d) f_2(c)\right), \tag{3}$$

where f_1 and f_2 are continuous and monotonic functions that vanish when their argument vanishes (in the Beer Lambert model f_1 and f_2 reduce to identity functions).

The function I_{norm} defined as

$$I_{\text{norm}} = \frac{\ln\left(\frac{I}{I_{\max}}\right)}{\ln\left(\frac{I_{\min}}{I_{\max}}\right)} = \frac{f_2(c)}{f_2(c_{\max})} \equiv f_3(c), \tag{4}$$

only depends on c, although the explicit form of f_3 is not known a priori. The determination of the latter is performed in practice through the auxiliary light calibration, measuring I_i and calculating $I_{\text{norm},i}$ for different pattern values c_i in the same range that the one employed in the displacement experiments. Then the variation of $I_{\text{norm},i}$ with c_i can be interpolated (typically by using a polynomial function of high degree) in order to obtain the analytical expression of c as a function of I_{norm} (i.e., f_3^{-1}). Finally, one can determine c by measuring I in the displacement experiments by using $c = f_3^{-1}(I_{\text{norm}})$. This procedure yields a solute concentration map $c(x, y, t)$ for each of these experiments.

2.3 Light transmission technique for suspensions

If we consider now the presence of macroscopic spherical particles in the layer of fluid in addition to the dissolved solute, the transmitted intensity I may depend not only on c, but also on the particle radius (a) and bulk volume fraction (ϕ_{bulk}). Although it is not straightforward to assume a monotonic variation of I with ϕ_{bulk} due to possible multiple light scattering effects, it is however plausible to assume that, at fixed a and ϕ_{bulk}, I will decrease monotonically and continuously with increasing c, because, in average, light paths within the suspension undergo an increasing absorption (see Figs. 1a–1d). If the optical size parameter $2a\pi/\lambda$ (λ is the light wavelength) is greater than five, then classical optics is suitable for describing light transmission in this situation. In our work this parameter takes a value of ∼100.

At the scale of the particles, I may fluctuate over different positions (x, y) over the layer as the local value of ϕ fluctuates, because particles in the light paths may distort local transmission. Consider however the situation of the layer being saturated homogeneously with suspension with a known c_i (e.g., Fig. 1b).

If the measured distribution of I_{norm} (and then that of c determined from it) over (x, y) is found to be stationary over length scales larger than a certain scale l_ϕ, then, above this scale, the influence of ϕ on I can be considered as an spatial average. Under this condition, it is possible to assign a representative value of I_i to c_i independently of the specific spatial organisation of the particles. The value of l_ϕ, that may a priori depend on ϕ_{bulk} and a, would be considerably larger than the particle or particle cluster sizes in order to smooth-out local ϕ fluctuations, but it should also be significantly smaller than l_c, the scale at which c varies along (x, y) in the displacement experiments. In other words, the determination of c from measured I can only be performed at a length scales greater than l_ϕ so that the influence of the particles is well captured by the spatial average.

In Section 4 we present the explicit relation between I_i and c_i for each of the combinations of ϕ_{bulk} and a used in the displacement experiments.

In Section 5 we analyse the stationarity of the measured spatial distribution of c and estimate the orders of magnitude of l_ϕ and of l_c for our experiments.

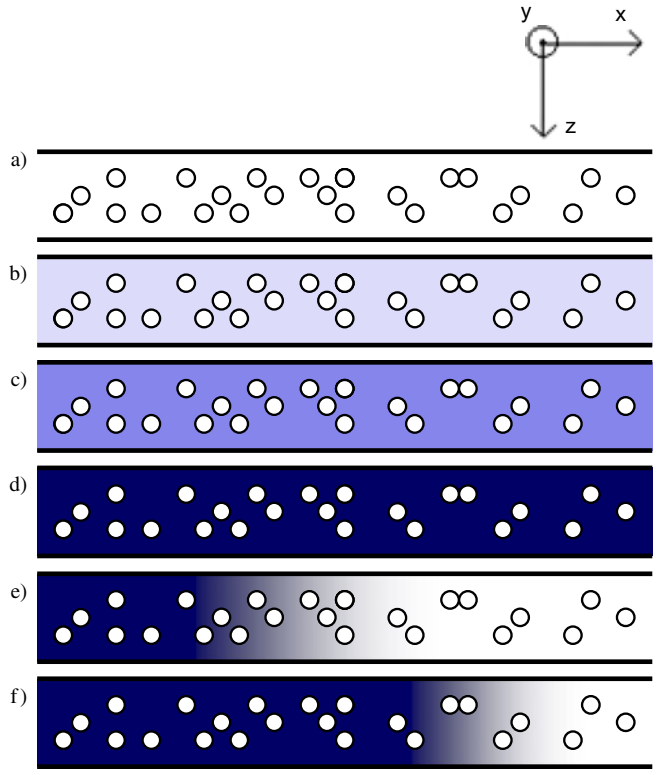

Fig. 1. (a–d) Schematics of the light calibration and (e–f) the displacement experiments. The cell contains a layer saturated homogeneously with (a) $c_i = 0$ g/L $= c_{\min}$, (b) $c_i = 0.4$ g/L, (c) $c_i = 1.2$ g/L, (d) $c_i = 2.0$ g/L $= c_{\max}$ g/L. (e, f) Evolution of the displacement front as the coloured suspension with $c_{\max}$ displaces the transparent one with $c_{\min}$.

Finally, for high values of ϕ_{bulk}, I is less dependent on c, due to the fact that particles (wherein there is no solute) occupy a large fraction of the total layer volume, and also in some conditions may block most of the transmission. In this case, the technique presented in this work may lack applicability.

2.4 Experimental device and procedure

In the displacement experiments, a transparent suspension, initially saturating the cell, is displaced by a suspension with a concentration $c_{\max}$ of a colouring solute (see Figs. 1e and 1f), until complete saturation by the latter. The experimental procedure for the displacement experiments (initial saturation of the cell, obtention of the initial condition corresponding to a straight sharp initial displacement front between the transparent and coloured suspensions, etc.) is identical to that reported in [28] and [29].

The Hele-Shaw cell, held horizontally in an aluminium frame, is made of two rectangular and parallel flat glass plates (25 cm × 10 cm × 1 cm). Two narrow mylar strips provided a constant separation between the two plates and sealed the longest sides of the cell (see Fig. 2) to allow axial flow between the inlet and outlet (two shorter sides of the cell). A fluid reservoir with an open top was attached to the inlet side of the cell; the outlet was connected through three Teflon tubes to a syringe pump sucking the suspensions out of the cell at a constant flow rate.

Images of the intensity transmitted through the cell, obtained with a 12-bit CCD camera, were acquired at constant time intervals. The cell aperture d was estimated from a comparison between the pump flow rate and the measured values of the mixing front mean velocity U (the velocity of the front of isoconcentration with $c/c_{\max} = 0.5$) in the displacement experiments, yielding 420 ± 10 μm.

These experiments were performed at mean flow velocities ranging between 0.040 and 0.051 cm/s (leading to $350 < Pe_{\text{s}} < 450$). The range of flow velocities (of Pe_{s}) and value of ϕ_{bulk} studied in this experiments were

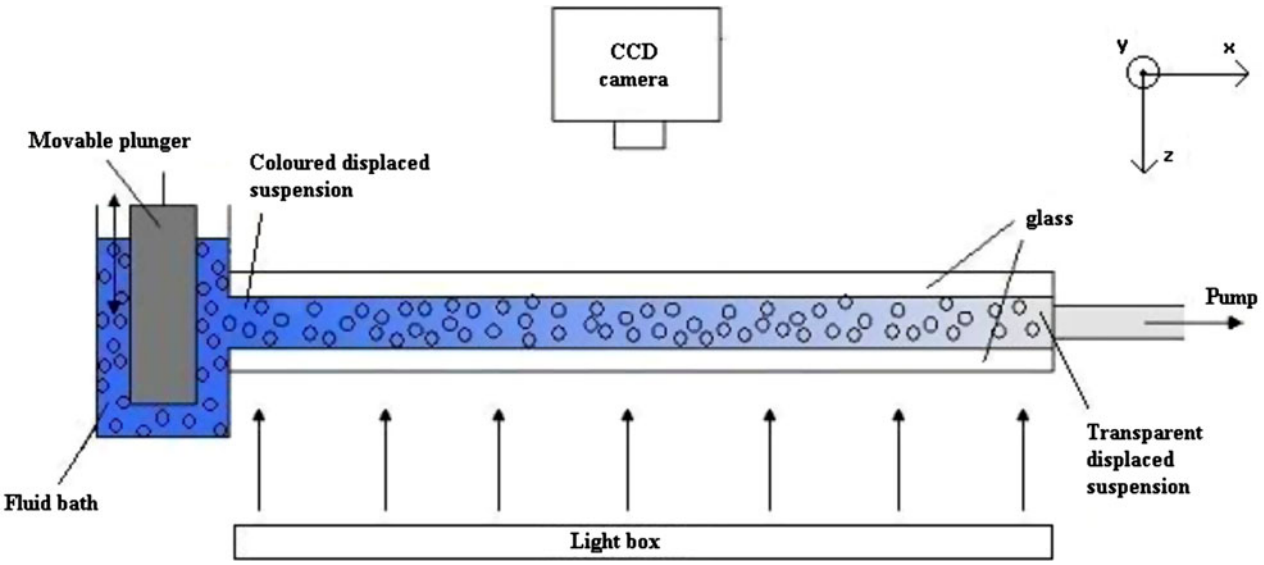

Fig. 2. Schematic view of the experimental setup. The coloured suspension displaces the transparent one at constant flow rate, while the camera acquires images of the transmitted intensity I through the cell.

chosen in view of the results of Roht et al. [15], that observed a variation in the dispersion coefficient of the solute due to the presence of the particles only for $Pe_s > 300$ and $\phi > 0.15$. Greater values of Pe_s may compromise the achievement of the Taylor dispersion in our 25 cm cell (making the cell too short), while as explained in Section 2.3 much higher values of ϕ_{bulk} may turn the light transmission technique inapplicable.

Depending on Pe_s, the duration of the experiments required to obtain complete saturation of the cell by the displacing fluid ranged between 1 h and 2 h (time interval between images from 55 s to 71 s). A total of 100 acquired images, with spatial resolution of 0.2 mm (1 pixel), were acquired during experiment.

Displacement experiments were performed for $\phi_{bulk} = 0.2$ ($a = 20$ μm) and $\phi_{bulk} = 0.2$ ($a = 40$ μm).

In addition to the displacement experiments with suspensions, a reference experiment and a light calibration, using exactly the same device assembly, were also performed.

Anytime a displacement experiment for $\phi_{bulk} = 0.2$ was performed, a reference experiment without particles (but otherwise identical) was also carried out in the same experimental conditions. This procedure allowed us to compare experiments with and without suspended particles, while keeping all the other parameters constant.

The light calibration is described in Section 2.5.

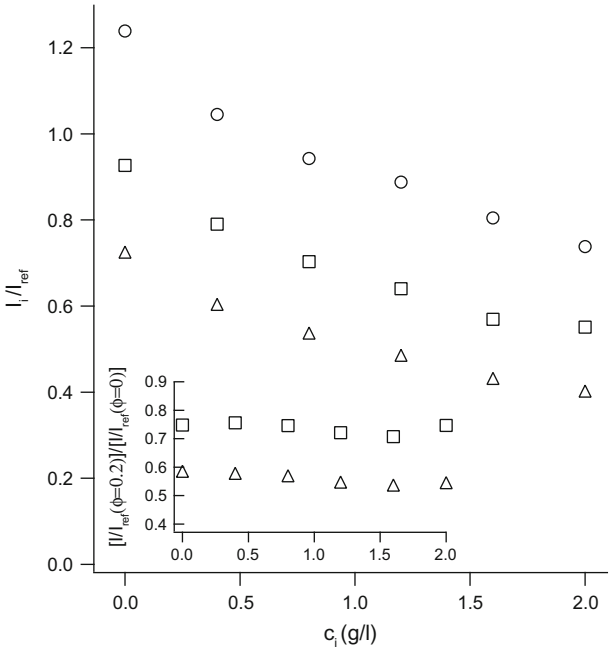

Fig. 3. Variation of I_i/I_{ref} as a function of c_i. (○): $\phi_{bulk} = 0$; (Δ): $a = 20$ μm, $\phi_{bulk} = 0.2$; (□): $a = 40$ μm, $\phi_{bulk} = 0.2$. The error bars are smaller than the symbols. Inset: Data series (Δ) and (□) divided by (○): the relative decrease of I_i due to the presence of the particles of a given size is rather constant with c.

2.5 Light calibration measurement

A light calibration measurement was performed independently for each displacement experiment.

The procedure consists in saturating the cell with fluid or suspensions with increasing pattern solute concentrations $c_i = 0$; 0.4; 0.8; 1.2; 1.6 and 2 g/L (Figs. 1a–1d).

The images of the transmitted intensity through the cell are acquired once two cell volumes of the fluid with c_i were injected, to ensure full saturation with it, and also, with the flow turned on, using a flow rate similar to that used in the displacement experiments. The latter is done to reproduce any flow-induced suspension microstructure that may arise in those experiments, affecting the light transmission (compared to the situation of null flow).

Also, in each calibration, the value of reference intensity (I_{ref}), in an external zone outside the cell was recorded in order to provide a reference to correct external lighting variations.

3 Image processing and data analysis

The time variation $c(x, y, t)$ for each point (x, y) in a measurement zone in the cell was fitted by the solution of the ADE equation to finally obtain a longitudinal Taylor dispersion coefficient D as detailed in references [28] and [15]. Both D and the dispersivity $l_d = D/U$ provide a quantitative measure of the degree of spreading of the mixing front between coloured and transparent suspension and then of the dispersion of the solute.

The measurement zone of dimensions (7.4 cm (x) by 4.6 cm (y)) is located near the outlet, far enough from the inlet in order to plausibly assume that both Taylor dispersion regime and suspension steady-state velocity profile are achieved (cf. Sect. 7). The characteristic time of solute transverse molecular diffusion in the cell aperture is $\tau_d = (d/2)^2/D_m$ and that corresponding to solute advection is $\tau_a = X_m/U$. The Taylor regime is achieved for a given X_m if $\tau_a \gg \tau_d$. Here U is the mean flow velocity, D_m the solute molecular diffusion coefficient X_m is the longitudinal position in the flow direction, and d is the cell aperture. In a typical experiment with $Pe_s = 450$ ($U = 0.0514$ cm/s, $D_m = 4.8 \times 10^{-6}$ cm^2/s (waterblue)), the above condition is satisfied near the outlet ($X_m = 25$ cm), having $\tau_d = 92$ s and $\tau_a = 486$ s. The Taylor regime can be then considered achieved in this case.

In Section 7, we discuss in quantitative terms the attainment of the suspension steady-state velocity profile in our experimental conditions.

4 Transmitted intensities

Figure 3 shows the variation of I_i/I_{ref} with c_i for $\phi_{bulk} = 0$ (carrier fluid only) and for $\phi_{bulk} = 0.2$ ($a = 20$ and 40 μm) in the auxiliary light calibration.

The values of I_i are normalized by I_{ref} (cf. Sect. 2.5) in order to correct external lighting variations between different series.

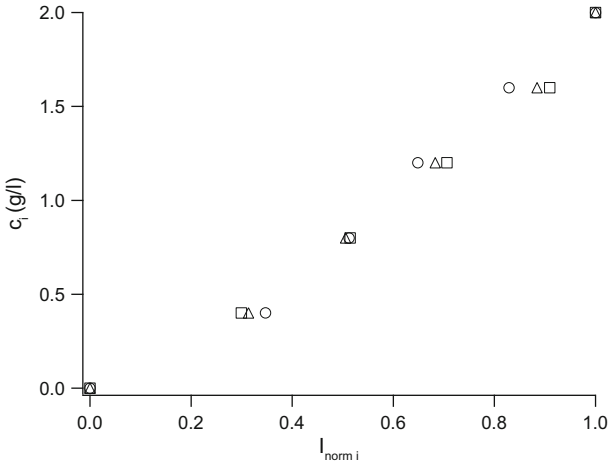

Fig. 4. Variation of c as a function of $I_{\mathrm{norm}i}$ (as defined in Sect. 2.2). ($\circ$): $\phi_{\mathrm{bulk}} = 0$; (Δ): $a = 20$ μm, $\phi_{\mathrm{bulk}} = 0.2$; ($\square$): $a = 40$ μm, $\phi_{\mathrm{bulk}} = 0.2$. A crossover in the behavior of $I_{\mathrm{norm},i}$ can be observed for $c_i = 0.8$. Error bars are omitted for clarity.

In Figure 3 we can observe that I_i/I_{ref} is lower for $a = 20$ μm than for $a = 40$ μm for all values of c_i. This would be consistent with the fact that, at a given ϕ_{bulk} and if no vertical overlap is assumed, the 20 μm particles (smaller but eight times more numerous at equal ϕ_{bulk}) present greater total cross section to the light than 40 μm ones, because the volume goes as a^3 but the cross section as a^2.

In the inset of Figure 3 we can see the values shown in Figure 3 for $\phi_{\mathrm{bulk}} = 0.2$ divided by the corresponding ones for $\phi_{\mathrm{bulk}} = 0$: the ratio is approximately constant for both particle sizes over all values of c_i.

From the figure one can infer that the resolution in the determination of c decreases as c increases, because the slope of I_i/I_{ref} with c_i decreases.

This can be also observed in Figure 4, where the variation of $I_{\mathrm{norm},i}$ (as defined in Sect. 2.2) with c_i is shown. There is a crossover near $I_{\mathrm{norm},i} \sim 0.5 (c \sim 0.8)$ for which the relative transmissivity for the three data series shown in Figure 3 is inverted.

The reader should have in mind that the normalization yielding I_{norm} (Eq. (4)) is performed separately for each of the datasets shown in the figure.

5 Concentration maps and profiles

Figure 5 shows maps of $c(x, y)$ (determined from the images of $I(x, y)$ following the procedure explained in Sect. 2.2) in the light calibration measurement, with the cell saturated with $c_i = c_{\mathrm{max}} = 2.0$ g/L, for $\phi_{\mathrm{bulk}} = 0$ ($\circ$), $\phi_{\mathrm{bulk}} = 0.2$ ($a = 20$ μm) (Δ) and $\phi_{\mathrm{bulk}} = 0.2$ ($a = 40$ μm) ($\square$). One can observe the appearance of a spatial correlation for $\phi_{\mathrm{bulk}} = 0.2$ (more pronounced for $a = 40$ μm), probably due to suspension microstructure affecting light transmission. A measure of the correlation length in the maps provides the length scale l_ϕ above which c becomes stationary and thus the one above which c can be representatively determined by the use of this technique (cf. Sect. 2.3). In the bottom-right subfigure we plot the correlation functions $\langle c(x_0, y_0)\, c(x_0, y_0 + \Delta y)\rangle$ (where Δy is the correlation lag and an ensemble-average is performed over all possible starting positions x_0, y_0) for the data series shown and fit them by decreasing exponentials to estimate l_ϕ from the characteristic decay length of the exponential.

This procedure yields $l_\phi = 72$ μm for $a = 20$ μm and $l_\phi = 101$ μm for $a = 40$ μm, while no correlation is observed for $\phi_{\mathrm{bulk}} = 0$.

Figure 5 shows the variation of c averaged in the width of the cell $\langle c(x, y)\rangle_y / c_{\mathrm{max}}$ as a function of the longitudinal position in the cell (distance from the inlet) for $t = 270$ s (aprox. 1/3 of the cell volume injected) in a displacement experiment with 40 μm particles ($\phi_{\mathrm{bulk}} = 0.2$) or without particles ($\phi_{\mathrm{bulk}} = 0$).

The lines represent a fit over the data points with the solution of the ADE equation for a fixed time and varying position x in the direction of the flow. From the plot we can see that the variation of $\langle c(x, y)\rangle_y$ with x is well represented by this solution in both cases. Also this variation is steeper for $\phi_{\mathrm{bulk}} = 0.2$ implying a lesser degree of solute dispersion.

Finally from these profiles we can estimate the characteristic length scale of solute spatial variation l_c to be O (cm), thus much greater than l_ϕ which was of O (10^2 μm). This supports the validity of the technique used (cf. Sect. 2.3), because at the scale l_c characterizing the solute variation, the influence of the spatial fluctuations of ϕ can be satisfactorily assumed to be smoothed-out (Fig. 6).

6 Solute dispersivity

In this section we present the results concerning the measurement of the solute dispersion coefficient D and dispersivity l_{d} as a function of Pe_{s} and a. As explained in Section 2.4, the choice of Pe_{s} and ϕ_{bulk} was made in view of the results of Roht et al. [15], that found a decrease of D in the presence of particles only for $\phi_{\mathrm{bulk}} > 0.15$ and $Pe_{\mathrm{s}} > 300$, while for $\phi_{\mathrm{bulk}} < 0.15$ and for $Pe_{\mathrm{s}} < 300$, $D(\phi_{\mathrm{bulk}} > 0)$ equaled $D(\phi_{\mathrm{bulk}} = 0)$ within the experimental error.

On the other hand, for $Pe_{\mathrm{s}} > 500$, measurements yielded solute concentration time variations $c(x, y, t)$ that weren't in agreement of the ADE solution, showing a predominant advective (non-diffusive) behavior in which it was not possible to define a dispersion coefficient.

Figure 7 shows the variation of D as a function of Pe_{s} for $\phi_{\mathrm{bulk}} = 0$ and $\phi_{\mathrm{bulk}} = 0.2$ ($a = 20$ μm and 40 μm). While no clear trend is observed for $Pe_{\mathrm{s}} = 350$, for $Pe_{\mathrm{s}} = 400$ and 450 a decrease of D is observed in the presence of particles in the flow ($\phi_{\mathrm{bulk}} = 0.2$) with respect to $\phi_{\mathrm{bulk}} = 0$: this decrease is more pronounced for the smaller particles and for increasing Pe_{s}.

The discrepancy between the theoretical prediction for the infinite parallel-plate configuration and our measurements (both for $\phi = 0$) may be due to the finite ratio

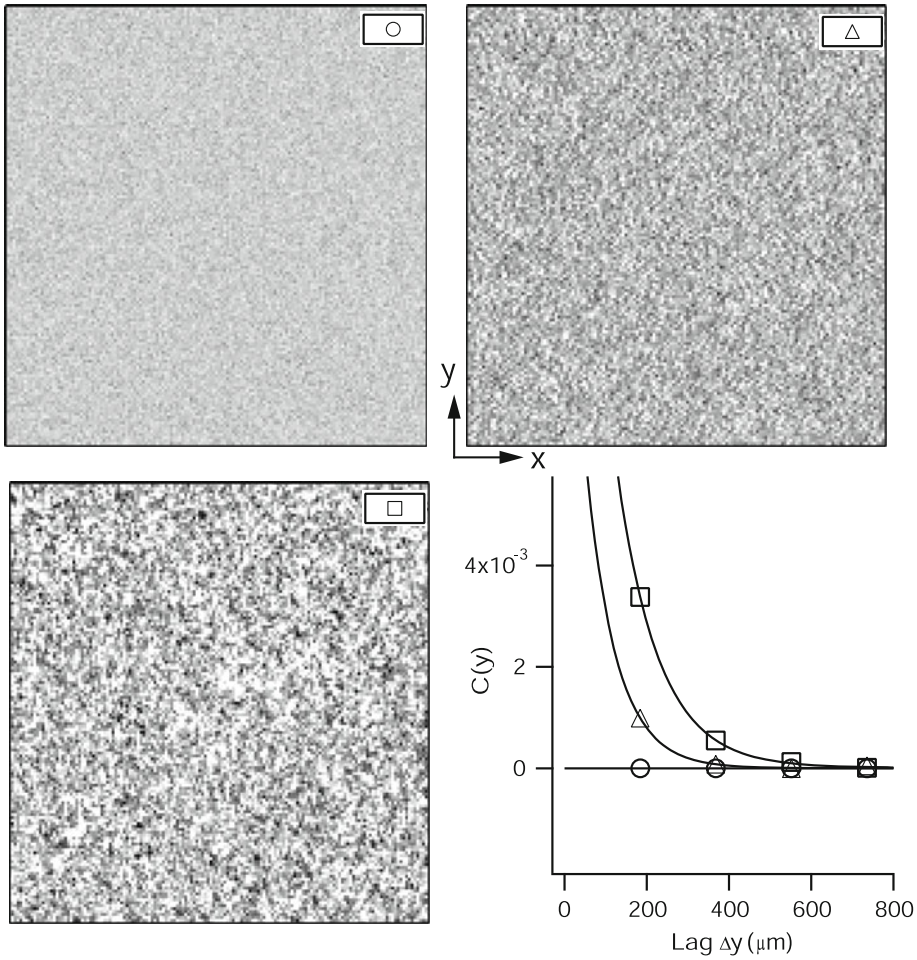

Fig. 5. Maps of measured $c(x,y)/c_{\max}$ obtained with the cell saturated with $c_i = c_{\max} = 2.0$ g/L. ($\circ$): $\phi_{\text{bulk}} = 0$; (Δ): $\phi_{\text{bulk}} = 0.2$, $a = 20$ μm, ; ($\square$): $a = \phi_{\text{bulk}} = 0.2$, 40 μm. White: $c/c_{\max} = 0.7$; black = $c/c_{\max} = 1.1$. The linear size of each map is 3 cm. Bottom-right: spatial correlation functions in the direction y for the three cases (symbols), with a decreasing exponential fit for each (full lines). The correlation appearing for $\phi_{\text{bulk}} = 0.2$ is presumably due to how suspension microstructure (cf. Sect. 2.3) modifies light transmission. The characteristic decay length of the exponential yields an estimate for l_ϕ in the order of 10^2 μm. Correlation functions for direction x show a similar behavior.

between fracture aperture and width (which has been shown theoretically [30] to increase the value of D relatively to the infinite parallel-plate configuration).

We intend to make the trend evident by plotting the values of D for $\phi_{\text{bulk}} = 0.2$ divided by those for $\phi_{\text{bulk}} = 0$ in Figure 8, where it can be observed that for $a = 20$ μm the relative decrease may reach 25%, while for $a = 40$ μm the decrease is always lower than 10%. Roht et al. [15] showed that the magnitude of this decrease, for fixed a, may increase with increasing ϕ_{bulk}.

Figure 9 shows the solute dispersivity $l_d = D/U$ as a function of Pe_s for $\phi_{\text{bulk}} = 0$ and $\phi_{\text{bulk}} = 0.2$ ($a = 20$ μm and 40 μm). As a reference, we plot a linear fit over data for $\phi_{\text{bulk}} = 0$ as suggested by equation (2), the slope of this fit is 0.0003 cm which yields an estimated value of d of 0.0063 cm that is of the order of magnitude of the measured cell aperture (see Sect. 2.4). This linear reference allows one to visualize the gap between behaviors for $\phi_{\text{bulk}} = 0$ and $\phi_{\text{bulk}} = 0.2$. Having in mind that particles introduce a second characteristic length-scale in the physical system under study, one could have expected a linear behavior in the dispersivity with a different slope (related not only to the cell aperture but also to the particle size (cf. Eq. (2)), but data points for $\phi_{\text{bulk}} = 0.2$ and in particular those for $a = 20$ μm hardly follow such a trend.

It has been demonstrated theoretically [31] that, in a flow of a colloidal suspension, the mean particle velocity might be higher than fluid one because, due to a finite-size exclusion effect, the (finite-sized) particles cannot sample the slowest flow lines. This result by other author shows that the appearance of a second characteristic length might indeed modify the solute dispersivity by affecting the flow properties.

7 Discussion and conclusions

A light transmission technique for measuring solute concentration in suspension flow was studied and characterized.

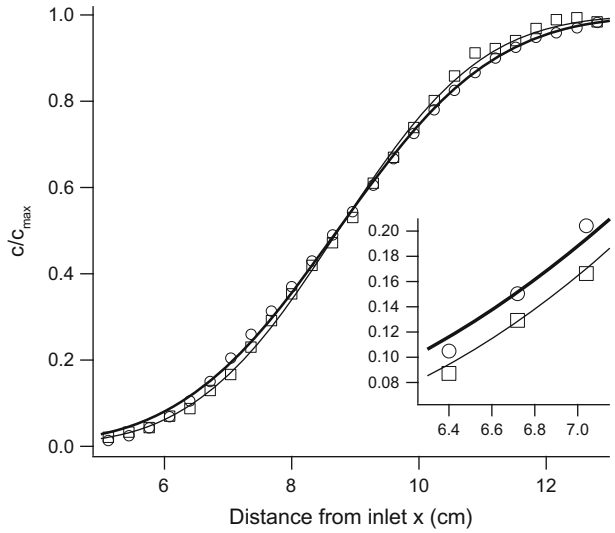

Fig. 6. Variation of $\langle c(x,y)\rangle_y$ as a function of the longitudinal position in the cell (x) (distance from the inlet) in a displacement experiment with $Pe_s = 450$ ($U = 0.0514$ cm/s). The profile corresponds to a time = 270 s, when approx. one third of the cell volume of transparent suspension (or fluid) has been injected. (○): $\phi_{bulk} = 0$. (□): $\phi_{bulk} = 0.2$, $a = 40$ μm. Thick and thin line: fits with the solution of the ADE model for (○) and (□) respectively. Inset: zoom over datapoints.

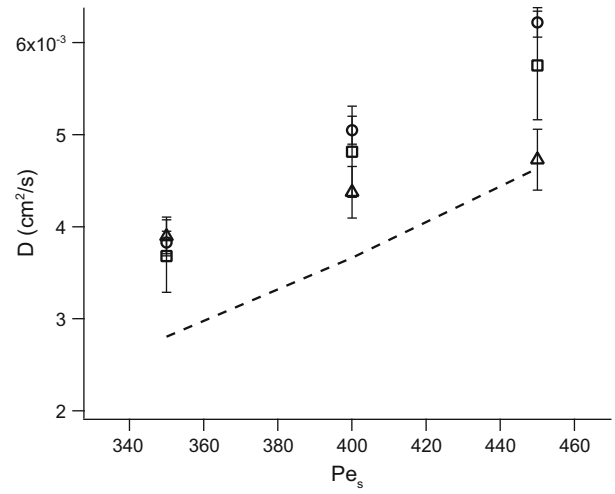

Fig. 7. D as a function of Pe_s(○): $\phi_{bulk} = 0$, (Δ): $a = 20$ μm, $\phi_{bulk} = 0.2$. (□): $a = 40$ μm, $\phi_{bulk} = 0.2$. The error bars indicate the width of the distribution of D values over (x,y) in the measurement zone. Dashed line: theoretical prediction for infinite parallel-plates ($\phi_{bulk} = 0$).

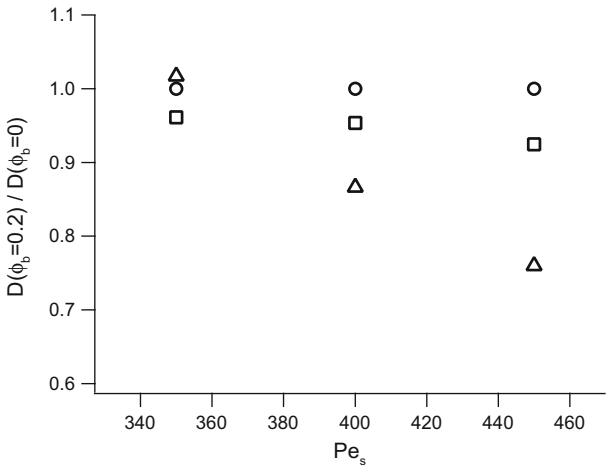

Fig. 8. D divided by D ($\phi_{bulk} = 0$) as a function of Pe_s. (○): $\phi_{bulk} = 0$ (as a reference). (Δ): $a = 20$ μm, $\phi_{bulk} = 0.2$. (□): $a = 40$ μm, $\phi_{bulk} = 0.2$. For clarity we don't include the error bars in this figure. The difference between the values for $\phi_{bulk} = 0$, $\phi_{bulk} = 0.2$ ($a = 20$ μm) and $\phi_{bulk} = 0.2$ ($a = 40$ μm) increases as Pe_s increases, with a clear trend.

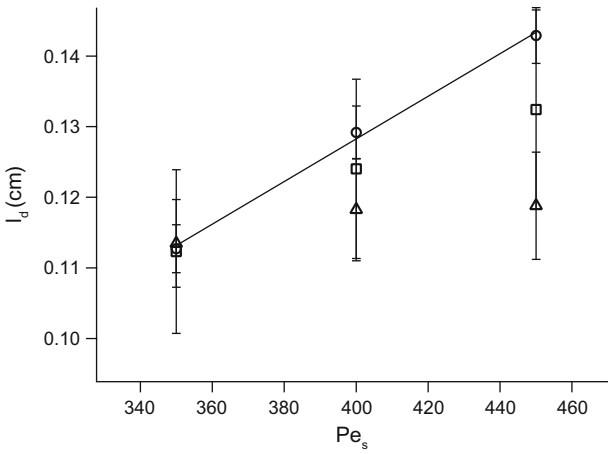

Fig. 9. Dispersivity l_d as a function of Pe_s. (○): $\phi_{bulk} = 0$. (Δ): $a = 20$ μm, $\phi_{bulk} = 0.2$. (□): $a = 40$ μm, $\phi_{bulk} = 0.2$. Line: linear fit over (○) following equation (2).

The validity of the technique was proposed to be subjected to the condition that the ratio between l_ϕ and l_c (cf. Sect. 2.3) is small enough so that a representative value of I_{norm} could be explicitly related to each pattern solute concentration c_i at fixed ϕ_{bulk} and a.

This condition was shown to hold in our experiments.

The results of the miscible displacement experiments between a coloured and a transparent suspension, for varying a and Pe_s, show that the decrease of D and l_d in the presence of particles in the flow is less pronounced for the larger particles.

With the definitions of Section 1.2 and using the values of the parameters corresponding to our experiments ($\mu_0 = 1.6$ cP, $a = 2$ or 4×10^{-5} m, $\dot{\gamma} = U_{max}/(d/2) = 3.6$ L/s, $T = 293$ K, $\rho_0 = 1.05$ g/cm^3) we can estimate Péclet and Reynolds numbers based on the particle size as $Pe_p = 2.18 \times 10^5$ and $Re_p = 0.0067$ ($a = 20$ μm) and $Pe_p = 1.74 \times 10^6$ and $Re_p = 0.026$ ($a = 40$ μm).

In these conditions, inertial and Brownian effects can be reasonably neglected for both particle sizes and hydrodynamic interactions are predominantly viscous. The physical reasons of the modification of D in the presence of particles should be sought mainly in the fact that the latter affect the flow velocity field.

The transition (or entrance) length L required to attain a steady state velocity profile due to particle migration in the flow of a suspension can be obtained by scaling laws [20]. These laws predict that $L/(d/2)$ scales as $((d/2)/a)^2$. Taking L as the distance from the inlet to the measurement zone used for analyzing our experiments, then $L/(d/2)$ is of order $O(10^3)$ while $((d/2)/a)^2$ is of $O(10^2)$, so the steady state for the suspension velocity profile can be considered attained. The choice of the measurement zone complies then simultaneously that the Taylor regime for the solute dispersion (cf. Sect. 3), and the steady state of the suspension velocity profile, are both a priori achieved. However, it is plausible to assume that the variation of the velocity profile, which is parabolic at the inlet and progressively flattens along the longitudinal axis of the cell, until the steady state is attained, might in turn affect the conditions of achievement of the Taylor dispersion regime. Nevertheless, the comparative scaling of the characteristic time of diffusion in the gap $\tau_\mathrm{d} = (d/2)^2/D_\mathrm{m}$ and that of solute advection $\tau_\mathrm{a} = X_\mathrm{m}/U$ would seem to be unaffected, provided the mean velocity U remains unchanged (in our experiments performed at constant flow rate this is the case).

The scaling law also predicts a higher migration rate (and thus a decrease in the transition length) as a increases.

Theoretical approaches such as the suspension balance model [20] or diffusive flux one [21] were able to predict the variation of the profiles of ϕ_bulk and of the velocity across the cell for varying ϕ_bulk. In particular, an increase of ϕ and a blunting or flattening of the velocity profile in the center of the cell aperture has been predicted numerically and verified experimentally [2].

The theories mentioned before do not describe the variation of the velocity profiles with a. However, results of Stokesian dynamics numerical simulations ([20], Sect. 4.2) showed that, as d/a ratio increases while ϕ_bulk is kept constant, the suspension velocity profile becomes more blunted.

On the other hand, in other types of flow such as that of a shear-thinning fluid (with no particles), it has been shown analytically and experimentally [32,33] that the flattening of the velocity profile implied a decrease of the dispersion coefficient D, mainly because the velocity gradient perpendicular to the main flow direction is reduced, and transverse diffusion, which is driven by this gradient, is less efficient.

In this order of ideas, the decrease of D for $\phi_\mathrm{bulk} = 0.2$ with respect to $\phi_\mathrm{bulk} = 0$ measured in our experiments would be consistent with the flattening of the velocity profile due to particle migration to low shear zones. With this in mind, our observation that such decrease is greater for smaller particles may be related to the numerical prediction that as a decreases, while d is kept constant, the velocity profile is more flattened and the velocity gradient across the cell is reduced. On the other hand, a dispersive effect, driven by the particle irregular motion resulting from multiparticle interactions, and scaling as $a^2\dot{\gamma}$, would impart an additional dispersive effect to the solute as well, to an extent that would be greater for the larger particles. Under this assumption, there would be a competition of the flattening of the velocity profile and this latter effect, the results presented here implying a stronger influence of the former one.

We find no theoretical explanation for the pronounced increase of the gap between D for $\phi_\mathrm{bulk} = 0.2$ and for $\phi_\mathrm{bulk} = 0$ with increasing Pe_s, since, as explained above in this section, Re_p is in all cases small and inertial effects should be negligible.

The results presented here are first results that derive as an application of a new experimental technique; further studies using a wider range and a more dense sampling of particle sizes and particle volume fractions should be conducted to establish a definitive trend of how the particle size influences solute dispersion. Also studies at the particle scale may shed light on the precise influence of the particle finite size on the suspension steady state velocity profile.

The authors would like to thank J.P. Hulin, L. Oger and G. Gauthier for fruitful discussions and remarks. This work was partially supported by the programs UBACYT 2002100100798, PIP 0246 and 1022 (Conicet).

References

1. M. Frank, D. Anderson, E. Weeks, J.F. Morris, J. Fluid Mech. **493**, 363 (2003)
2. R.E. Hampton, A.A. Mammoli, A.L. Graham, N. Tetlow, S.A. Altobelli, J. Rheol. **41**, 621 (1997)
3. G. Ovarlez, F. Bertrand, S. Rodts, J. Rheol. **50**, 259 (2006)
4. G. Drazer, J. Koplik, B. Khusid, A. Acrivos, J. Fluid Mech. **511**, 237 (2004)
5. T.S. Lo, J. Koplik, Phys. Fluids **24**, 053303 (2012)
6. National Academy of Sciences, *Rock fractures and fluid flow: Contemporary understanding applications* (National Academy Press, Washington, DC, 1996)
7. V.J. Charette, E. Evangelista, R. Chertcoff, H. Auradou, J.P. Hulin, I. Ippolito, Eur. Phys. J. Appl. Phys. **39**, 267 (2007)
8. D.L. Koch, J.L. Brady, J. Fluid. Mech. **154**, 399 (1985)
9. H. Auradou, G. Drazer, J.P. Hulin, J. Koplik, Water Resour. Res. **41**, W09423 (2005)
10. A. Boschan, H. Auradou, I. Ippolito, R. Chertcoff, J.P. Hulin, Water Resour. Res. **45**, W03201 (2009)
11. N. Massei, M. Lacroix, H.Q. Wang, J.P. Dupont, J. Contam. Hydrol. **57**, 21 (2002)
12. O. Zvikelsky, N. Weisbrod, Water Resour. Res. **42**, WR004873 (2006)
13. M.D. Reno, S.C. James, S.J. Altman, J. Colloid Interface Sci. **300**, 383 (2006)
14. Q. Zheng, S.E. Dickson, Y. Guo, J. Colloid Interface Sci. **339**, 140 (2009)
15. Y.L. Roht, A. Boschan, I. Ippolito, R. Chertcoff, J. Contam. Hydrol. **145**, 10 (2013)
16. J. Bear, *Dynamics of Fluids in Porous Media*, edited by Dover Publications Inc. (American Elsevier Publishing, New York, 1972), p. 784
17. R. Aris, Proc. Roy. Soc. A **235**, 67 (1956)

18. M.J.E. Golay, Gas Chromatography (Butterworths, London, 1958)
19. S. Roux, F. Plouraboué, J.P. Hulin, Transp. Porous Media **32**, 97 (1998)
20. P.R. Nott, J.F. Brady, J. Fluid Mech. **275**, 157 (1994)
21. R.J. Phillips, R.C. Armstrong, R.A. Brown, A.L. Graham, J.R. Abbott, Physics of Fluids A: Fluid Dyn. **4**, 30 (1992)
22. J.J. Stickel, R.L. Powell, Annu. Rev. Fluid Mech. **37**, 129 (2005)
23. G. Drazer, J. Koplik, B. Khusid, A. Acrivos, J. Fluid Mech. **460**, 307 (2002)
24. D. Leighton, A. Acrivos, J. Fluid Mech. **181**, 415 (1987)
25. M.K. Lyon, L.G. Leal, J. Fluid Mech. **363**, 57 (1998)
26. K. Yapici, R.L. Powell, R.J. Phillips, Phys. Fluids **21**, 053302 (2009)
27. R.W. Horobin, J.A. Kiernan (Eds.), *Conn's Biological Stains*, 10th edn. (Bios Scientific Publishers, Oxford, 2002)
28. A. Boschan, H. Auradou, R. Chertcoff, I. Ippolito, J.P. Hulin, Water Resour. Res. **43**, W03438 (2007)
29. A. Boschan, I. Ippolito, R. Chertcoff, H. Auradou, J.P. Hulin, Water Resour. Res. **44**, W06420 (2008)
30. P.C. Chatwin, P.J. Sullivan, J. Fluid Mech. **120**, 347 (1982)
31. S.C. James, C.V. Chrysikopoulos, J. Colloid Interface Sci. **263**, 288 (2003)
32. M. Vartuli, J.P. Hulin, G. Daccord, AICHE J. **41**, 1622 (1995)
33. A. Boschan, J. Charette, S. Gabbanelli, I. Ippolito, R. Chertcoff, Physica A **327**, 49 (2003)